An Extreme Wave Event in eastern Yucatán, Mexico: evidence of a paleotsunami event during the Mayan times

Javier Lario[1], Chris Spencer[2], Teresa Bardají[3], Ángel Marchante[4], Victor H. Garduño-Monroy[5], Jorge Macias[6], Sergio Ortega[7].

1. Facultad de Ciencias, UNED, Spain. e-mail: javier.lario@ccia.uned.es

2. Geography and Environmental Management, UWE, Bristol, UK

3. Departamento de Geología, Geografía y Medio Ambiente, Universidad de Alcalá, Spain.

3. Grupo de Investigación TARHA, Universidad de las Palmas de Gran Canaria, Spain.

5. Departamento de Geología y Mineralogía, Universidad Michoacana de San Nicolás de Hidalgo, México.

6. Depto. de A.M., E. e I.O. y Matemática Aplicada, Facultad de Ciencias, Universidad de Málaga, Spain.

7. Laboratorio de Métodos Numéricos, SCAI, Universidad de Málaga, Spain.

ABSTRACT

The Yucatán Peninsula, Mexico, has typically been considered a tectonically stable region without significant seismic activity, in contrast, the region is one that is regularly affected by hurricanes. A detailed survey of ca. 100 km of the eastern Yucatan and Cozumel coast identified the presence of ridges containing individual boulders measuring >1 m, with up to three ridges at some locations. The ridges reach five metres in height and their origin is associated with Extreme Wave Event (EWE) activity. Previously modelled tsunami waves from known seismically active zones in the region (Muertos Thrust Belt and South Caribbean Deformed Belt) are not of sufficient scale in the area of the Yucatan peninsula to have produced the boulder ridges recorded in this study. The occurrence of hurricanes in this region is more common, but two of the most destructive (Hurricane Gilbert 1988 and Hurricane Wilma 2005) produced coastal waves too small to have created the ridges recorded here. In this paper, a new tsunami model has been generated that indicates a tsunami event may have caused the EWE that resulted in the deposition of the boulder ridges.

Key words: Extreme Wave Event, tsunami, boulders, paleoseismology.

INTRODUCTION

The Yucatan Peninsula of Mexico is a carbonate platform comprised of Eocene-age limestone in the interior, with off-lapping sequences to a Quaternary coastline (Weidie, 1985). The present-day coastline is incised into the Pleistocene shelf margin, reef, and back-reef limestones, which were deposited during the last interglacial sea level highstand (marine

isotope stage -MIS 5). The Pleistocene deposits extend inland for some 10 km and form the most recent of a sequence of accreted carbonate units reaching at least 12 m thick (Ward, 1985).

The Peninsula is considered to have been tectonically stable since the late Pleistocene (Szabo et al., 1978), this belief is also supported by the lack of recorded historical seismicity (Marquez-Azua et al., 2004).

A detailed survey of ca. 100 km of the eastern Yucatan coast (Quintana Roo and Cozumel Island) identified the presence of beach ridges comprised of individual boulders measuring >1 m (Figure 1). The ridges reach five metres in height and their origin is inferred to be associated to Extreme Wave Event (EWE) activity, either tsunamis (not recorded as having occurred in the area) or hurricanes (frequently recorded in the area). These boulder ridges were recently partially described by Shaw and Benson (2015) and associated to a tsunami event, but no evidence of the tsunami source was provided.

BOULDER RIDGES

There are two main areas where boulder ridges were studied in detail: the coast in Quintana Roo between Playa del Carmen and Caleta Tankah and the eastern coast of Cozumel Island (Figure 1).

The ridges are composed of accumulations of coral reef boulders, most of them imbricated. Individual boulders are more than 1 m length and the ridges reach heights of 5 m. Accumulations of boulders are more extensive along more rocky sections of the coastline, rocky platforms and capes, whilst in caletas (karstic bays) the boulder ridges are absent instead a ridge of sand, reef pebbles and cobbles is present. Typically, the boulders originate from joint bounded blocks (JBB) originally forming part of the late Pleistocene platforms near msl. At some of the sites a second smaller ridge exists overlapping the main one, the smaller ridges are typically composed of pebbles and cobbles.

More than 100 boulders have been measured (a, b and c dimensions, height, distance to the sea and main lithology) and photographed for photogrammetry using Agisoft Photoscan software (Agisoft, 2017). As a result of the photogrammetry a 3D reconstruction of the boulders was created and all of the dimension can be calculated from them. Thus, the volume of these boulders can be measured accurately (Figure 2). The blocks and boulders represent heterogeneous reef-rock and consist of varying percentages of several different lithofacies. The bulk density of similar deposits has been determined to be between 2.07-2.40 g/cm^3 by Engel and May (2012).

MODELLING BOULDER TRANSPORT

Several studies have tried to infer the height of wave required to transport boulders at the coast. Nott (1997 2003), assert that the pre-transport situation of a coastal boulder, relative to mean water level, along with its shape, size and density determines the height of wave required for it to be transported. Therefore, the Nott (2003) studies presented formulas to calculate the height of wave required to move boulders by both tsunami and storm waves in three different pre-transport situations: submerged boulders, sub-aerial boulder and joint

bounded blocks. Noormets et al. (2004) noted that tsunami waves have a considerably longer wave period than storm waves, and thus, may have greater transporting capacities because each wave has the potential to transport blocks for a longer time than a storm wave. Indeed, storm waves can break and emplace megaclasts but they tend to attenuate faster than tsunami waves. Pignatielli et al. (2009) introduced some modifications to Nott´s (2003) formulas to incorporate the fact that the boulder has one side facing the wave and one top surface and is limited by four sides. Later Barbano et al. (2010) also modified this proposal after testing the wave transport equations on the coast of Sicily. Nandasena et al. (2011) improved Nott´s equations further and found that the minimum flow velocity required to initiate the transport of submerged boulders from the revised equation was less than that from Nott's equations (e.g. reduced wave height required by up to 56% for submerged boulders and 65% for joint bounded blocks). Also, they developed a "boulder transport histogram" to represent the range of flow velocity that satisfies the requirements for initial transport of a boulder via different modes of transport: sliding, rolling, and saltation. This boulder transport histogram can be used to predict the possible initial transport modes of a boulder from the flow velocity. Engel and May (2012) reviewed and applied the Nandasena et al. (2011in Bonaire (Caribe) and the results indicated that boulder weight and dimension, and thus calculated wave energy and wave heights were overestimated in most of the previous studies. Also, as Spiske et al. (2008), they concluded that realistic bulk densities are critical for inferring minimum storm and tsunami wave heights from the boulder record.

Height of the extreme wave

Taking into account all of these formulas, and because most of the boulders examined in this study correspond to a JBB scenario, the equations below have been utilised:

Nott (2003) proposal for JBB scenario, where:

$$Ht \geq \frac{0.25\,(\frac{\rho b - \rho w}{\rho w})a}{C_L}$$

$$Hs \geq \frac{(\frac{\rho b - \rho w}{\rho w})a}{C_L}$$

where *Ht*= height of tsunami wave; *Hs*= height of storm wave; C_L=coefficient of lift=0.178; a= A axis of boulder; *ρb* = density of boulder; *ρw*= density of sea water= 1.02 g/ml.

The proposal of Engel and May (2012) based on the modifications to Nott by Nandasena et al. (2011) for JBB scenario, where:

$$Ht = \frac{(\rho b - \rho w) \cdot V \cdot (\cos\theta + \mu \cdot \sin\theta)}{2 \cdot \rho w \cdot C_L \cdot a \cdot b \cdot q}$$

$$Hs = \frac{(\rho b - \rho w) \cdot V \cdot (\cos\theta + \mu \cdot \sin\theta)}{0.5 \cdot \rho w \cdot C_L \cdot a \cdot b \cdot q}$$

where *V*=corrected boulder volume; *q*=boulder area coefficient 0.73; b=B axis of boulder; μ=coefficient of static friction 0.65; θ=angle of the bed slope of the pre-transport setting.

Table 1 presents the results from the main characteristic boulders (by weight, distance to the sea or altitude). The results using the Engel and May (2012) proposal for JBB scenarios demonstrated that to move the heaviest and largest boulders the height of a tsunami wave would need to be between 2.0 and 2.9 m. In addition, the height of storm wave must be between 8.0 and 11.5 m. Using the Nott (2003) formulas for the same scenario the results in general show an underestimation of the wave height in both cases.

Flow velocity and flow depth required to move the boulders

For the "boulder transport histogram" introduced by Nandasena et al. (2011) in the case of a submerged or subaerial boulder, transport begins with sliding and

$$u^2 \geq \frac{2(\rho b/\rho w - 1)gc(\mu_s \cos\theta + \sin\theta)}{C_d(c/b) + \mu_s C_L}$$

when transport begins with rolling (overturning),

$$u^2 \geq \frac{2(\rho b/\rho w - 1)gc(\cos\theta + (c/b)\sin\theta)}{C_d(c^2/b^2) + C_L}$$

when transport begins with saltation,

$$u^2 \geq \frac{2(\rho b/\rho w - 1)gc\cos\theta}{C_L}$$

in the case of a joint-bounded block, transport begins with lifting,

$$u^2 \geq \frac{2(\rho b/\rho w - 1)gc(\cos\theta + \mu_s \sin\theta)}{C_L}$$

where u is the flow velocity, g is the gravitational acceleration (9.81 m/s^2), μ_s is the coefficient of static friction between the boulder and the bed (0.7), C_d is the coefficient of drag (1.95) (Nandasena et al., 2011; 2014).

To estimate the flow depth from the minimum flow velocity required to move the boulder Nandasena et al. (2014) proposed a relationship between flow depth and flow velocity described by the Froude number as $Fr = u/\sqrt{gh}$, where h is the flow depth. The Froude number for past tsunamis has been determined as between 0.7 and 2.0, in this study the values 1.0 and 1.5 were used as proposed by Nandasena et al., (2012, 2014).

Table 2 presents the results applying these formulas to the main characteristics of boulders examined in this study (weight, distance to the sea or altitude) and Figure 3 presents the "boulder transport histogram" for these same boulders.

Table 2 and figure 3 display the minimum flow velocity and range of flow velocities to initiate boulder transport at each site. The average results display not less than 3.0 m/s at the pre-transport location of the boulders prior to the EWE. If the average flow velocity was higher than 3.0 m/s, the boulders would have been transported by sliding. If the average flow velocity was higher than 4.3 m/s, the boulders would have been transported by rolling, higher than 9.1 m/s by saltation and, in the situation of JBB, as is the case, higher than 9.3 m/s by lifting.

Table 2 also indicates the flow depth necessary to initiate boulder transport using the models applied here. Nandasena el al. (2014) indicate the difficulty in establishing the Froude number at each site. With the proposed F_r=1.0 the minimum flow depth to initiate the transport by sliding ranges from 0.4-2.1 m (average 1.0 m), by rolling 0.6-5.3 m (average 2.1 m), by saltation 2.6-16.5 m (average 8.8) and by lifting, as is the case for JBB, the flow depth must be between 2.7 and 17.1 m (average 9.1 m). With F_r=1.5 the minimum flow depth to initiate the transport by sliding ranges between 0.2-0.9 m (average 0.4 m), by rolling 0.2-2.3 m (average 0.9 m), by saltation 1.2-7.3 m (average 3.9 m). By lifting the minimum flow depth ranges between 1.2 and 7.6 m (average 4.0 m), a value more applicable to the boulder ridges recorded in this study.

TSUNAMI VS. HURRACAINE ORIGIN

Seismicity and hurricanes in Yucatan

The Yucatan Peninsula is considered a tectonically stable area at least since the late Pleistocene (Szabo et al., 1978). The Mexican Seismic Service (SSS, 2018) has only registered four earthquakes in the Yucatan Peninsula since 1990, and all with Mw lower than 4.6. Tsunami catalogues in the Caribbean area show no recorded events for the Quintana Roo coast (compiled in Engel et al., 2016). The tsunamigenic earthquakes in the Caribbean Plate are mostly concentrated along the western (Lesser Antilles), north-western (Muertos Thrust Belt) and south-western (South Caribbean Deformed Belt) plate boundaries (NOAA, 2018). However, models of tsunami propagation (Engel et al., 2016) show that a tsunami generated by a Mw 7.9 earthquake from the Muertos Thrust Belt (MTB) cannot reach the Yucatan coast. Moreover, a tsunami triggered by a Mw 8.8 earthquake from the South Caribbean Deformed Belt (SCBD) would reach the north-eastern Yucatan coast with a wave height <1.0 m, thus not high enough to produce the boulder ridges investigated in this study.

A different source of seismic activity is required, therefore, generate a tsunami wave able to reach the eastern coast of Yucatan and thus, to confirm the tsunami origin for these boulder ridges. Two recent events off coast of Honduras (Mw7.3, 2009 and Mw7.6, 2018; USGS, 2018) and a third one in Guatemala (Mw7.5, 1976; USGS, 2018) are associated to the Motagua/Swan Island Fault System (MSFS), identifying this as a possible source for a tsunamigenic earthquake. Likewise, two late Holocene M>7 earthquakes, have been also reported by Cox et al., (2008) before the occurrence of the 2009 and 2018 events, leading these authors to propose a 1000 yr recurrence interval for large earthquakes (Mw>7) associated with the MSFS.

The MSFS is a left-lateral strike-slip fault, segment of the boundary between North America and Caribbean plates, which accommodates about 20mm/yr slip (USGS, 2018). However, the instrumental and paleoseismic earthquake records presented above indicate that despite the relatively low slip rate of the MSFS, the resulting seismic and tsunami potential can be significant.

The occurrence of hurricanes in this region is more common, and Yucatan Peninsula is exposed to an average of 20 tropical cyclones each 150 year (Rosengaus Moshinsky et al., 2014). In order to characterize the extreme wave climate and storm surge in the Mexican Pacific Ocean and Gulf of Mexico/Caribbean Sea, Meza-Padilla et al. (2015) modelled a total of 3100 synthetic events achieving landfall in Mexico (divided between both basins) and found that the highest waves are expected in the Mexican Caribbean and the northern coast of the Gulf of Mexico whilst the highest storm surge is in the northern part of the Yucatan Peninsula. Two of

the most destructive hurricanes to have made landfall in the Eastern Yucatan produced 4-8 m high waves at the coast and inundation up to 5 km inland (Hurricane Gilbert, 1988, Rosengaus Moshinsky and Sánchez Sesma, 1990) and 8-10 m high waves at the coast (Hurricane Wilma, 2005, Alva González, 2015), however coastal waves of this scale are still too small to have produced the ridges recorded in this study.

Modelling a tsunami in eastern Yucatan Peninsula

A model of a tsunami generated by a seismic event from the Motagua fault has been generated simulating an earthquake Mw 7.6, 19 km depth with a 110 km length and 26 km width rupture area. The numerical code used is Tsunami-HySEA, this is a GPU-based shallow water code, developed by the EDANYA Group (University of Málaga) and extensively benchmarked for tsunami simulations (Macías et al., 2017). For the numerical simulation, a two-way nested mesh technique (as in Macías et al., 2016) is used. The global mesh that covers the computational domain has a resolution of 15 arc sec (~450m). Then six nested meshes, with an enhanced resolution of 0.9375 arc sec (~28 m) are used in the coastal strip to better assess tsunami wave height in this region.

Results at x32 resolution show that a wave height ca. 2.0 m would be generated in the studied area (Figure 4). Therefore, it is reasonable to assign the main boulder ridge to a tsunami generated by an earthquake Mw > 7.6 offshore in the eastern Caribbean sector of the Motagua fault. The smaller ridge overlapping the main boulder ridge was generated by the Hurricane Wilma in 2005 (witness's communication), demonstrating that destructive Hurricanes do not have sufficient energy in this area to generate the large boulders ridges recorded.

Appling the proposed intensity scale of Tsunami Environmental Effects (TEE-16 Scale, Lario et al., 2016), the tsunami intensity observed in the study area would be VI-VII (slightly damaging-damaging), but this is not the maximum intensity because the area is some considerable distance from the source.

Tsunami age and paleoseismic implications

Dating of wave-emplaced blocks and boulders is still a challenge (Terry et al., 2013; Engel et al., 2016; Rixhon et al., in press). Also, the coral ridges and single boulders recorded in this study may have a complex, long-term history of transport, accumulation, and modification during several strong storms and tsunamis (Morton et al., 2008; Scheffers et al., 2014; Rixhon et al., in press). Therefore, it is a challenge to provide a definitive date for the boulder emplacement in the ridges without finding shells, such as *lithophaga,* attached to the boulders prior to their transportation. Shaw and Benson (2015) recorded and dated peat deposits beneath the boulder ridge in the Akumal area and so pre-dating the main boulder ridge near Akumal. ^{14}C dating provides 2σ calibrated ages for two samples (1390–1567 and 1348–1613 cal YBP) suggesting that the tsunami event took place between ca.500-800 AD, during the late Classic period. In some locations within the region, it is possible observe Mayan buildings constructed over and therefore post-dating, the boulder ridges, for example in the Xcaret complex or Punta Chile (SW XpuHa, Figure 5). Despite the different phases of construction, these remains are Costa oriental in style (Eastern coast), meaning post classic Maya period, between 900-1521 AD (Andrews and Andrews, 1975: Covarrubias and Rojas, pers.comm,). This reinforces the date of the event as being between 500-900 AD. It is remarkable that there is no evidence of settlements prior to the post-classic period in this coastal area, and it may be that any small settlements that did exist were affected and covered by the tsunami deposits. This is also

supported by Cox et al., (2008) who found evidence of a large earthquake Mw>7.0 triggered in the MSFS in 900 AD in uplifted coral reef platforms, the event affected at least the north coast of Honduras.

The confirmation of a likely tsunami event caused by a Mw>7.6 earthquake on the Motagua fault implies that even if a long recurrence interval exists, destructive tsunami episodes can reach the eastern Yucatan coast. Despite the belief that the area has been tectonically stable since the late Pleistocene this study found more evidence of seismic activity during Mayan times, such as archeoseismological features located in Mayan sites (tilted walls, "antiseismic" fabric…), evidence of seismic events in submerged caves systems (tilted speleothems, collapses and orientated speleothems…) as well as faults affecting the late Pleistocene and Holocene reef deposits (eastern Cozumel), that are still being investigated (Lario et al., 2017).

CONCLUSIONS

A semi-continuous boulder ridge up to 5 m a.s.l, has been recorded on the eastern coast of the Yucatan Peninsula and Cozumel Island, generated by an Extreme Wave Event. The application of different approaches demonstrates that waves of between 2.0-2.9 m (in the case of a tsunami origin) and between 8.0-11.5 m (in the case of storm/hurricane origin) would need to be generated to result in the accumulation of these boulder ridges. Most of the possible tsunami source areas located in East Caribbean are not capable of generating a tsunami that would reach the Yucatan coast. However, as demonstrated through model simulation in this study, the Motagua Fault section located in the SW Caribbean basin can generate a tsunami with waves of between 2.0-3.0 m height at the eastern Yucatan coast, resulting from an earthquake of >Mw 7.6.

This and other evidence, demonstrates the occurrence of seismic activity during late Pleistocene and Holocene in the Eastern Yucatan Peninsula and surrounding areas illustrating the necessity to review all mitigation protocols in this area related to seismic and tsunami hazards.

Acknowledgements: Financial support by Spanish government projects CGL2013-42847-R and CGL2015-69919-R and SIMURISK (MTM2015-70490-C2-1-R). The GPU and multi-GPU computations have been performed at the Unit of Numerical Methods (UNM) of the Research Support Central Services (SCAI) of the University of Malaga. It is a contribution to the GTE IGCP Project 639 "Sea Level Change from Minutes to Millennia".

REFERENCES

Agisoft (2017). Agisoft PhotoScan User Manual. Professional Edition, Version 1.3, San Petersburgo.

Alva González, O.J. (2015). Evaluación de daños en la infraestructura de los estados de Quintana Roo y Yucatán causados por el huracán Wilma de 2005. Tesis de Licenciatura, Facultad de Ingeniería, UNAM, 84 pp.

Andrews, E.W. and Andrews, A.P. (1975). A preliminary study of the ruins of Xcaret, Mexico, with notes on other archaeological remains on the central east coast of the Yucatan Peninsula. Middle American Research Institute, Publication 40, Tulane University, New Orleans, 117 pp.

Cox, R., Lumsden, D.,Gough, K., Lloyd, R. and Talnagi, J. (2008). Investigation of late Quaternary fault block uplift along the Motagua/Swan Islands fault system: Implications for seismic/tsunami hazard for the Bay of Honduras. *Tectonophysics*: **457**, 30-41.

Engel, M., and May, S.M. (2012). Bonaire's boulder fields revisited: evidence for Holocene tsunami impact on the Leeward Antilles. *Quaternary Science Reviews*, **54**, 126-141.

Engel, M., Oetjen, J., May, S.M. and Brückner, H. (2016). Tsunami deposits of the Caribbean – Towards an improved coastal hazard assessment. *Earth-Science Reviews,* **163**, 260-296.

Lario, J., Spencer, C., Bardají, T., Marchante, A., Garduño-Monroy, V.H., Macias, J. and Ortega, S. (2017). An Extreme Wave Event in eastern Yucatán, Mexico: evidence of a paleotsunami event during the Mayan times. Proceedings of the 8th International INQUA Meeting on Paleoseismology, Active Tectonics and Archeoseismology. Lower Hutt (NZ): GNS Science: 38-41p. (*GNS Science miscellaneous series* **110**).

Lario, J.; Bardají, T.; Silva, P.G.; Zazo, C.; Goy, J.L. (2016). Improving the coastal record of tsunamis in the ESI-07 scale: Tsunami Environmental Effects Scale (TEE-16 scale). *Geologica Acta*, **14**, 179-193.

Macías, J., Castro, M.J., Ortega, S., Escalante, C. and González-Vida, J.M. (2017). Performance benchmarking of Tsunami-HySEA model for NTHMP's inundation mapping activities. *Pure and Applied Geophysics*, **174**, 3147–3183.

Macías, J., Mercado, A., González-Vida, J.M., Ortega, S. and Castro, M.J. (2016). Comparison and numerical performance of Tsunami-HySEA and MOST models for LANTEX 2013 scenario. Impact assessment on Puerto Rico coasts. *Pure and Applied Geophysics*, **173**, 3973–3997.

Márquez-Azua, B., Cabral-Cano, E., Correa-Mora, F. and DeMets, C. (2004). A model for Mexican neotectonics based on nationwide GPS measurements, 1993–2001. *Geofisica Internacional*, **43**, 319–330.

Meza-Padilla, R.; Appendini, C.M. and Pedrozo-Acuña, A. (2015). Hurricane-induced waves and storm surge modeling for the Mexican coast. *Ocean Dynamics*, **65**: 1199–1211.

Morton, R.A., Richmond, B.M., Jaffe, B.E., Gelfenbaum, G. (2008). Coarse-clast ridge complexes of the Caribbean: a preliminary basis for distinguishing tsunami and storm-wave origins. *J. Sediment. Res.*, **78**, 624-637.

Nott, J. (2003). Waves, coastal boulder deposits and the importance of the pretransport setting. *Earth Planet. Sci. Lett.*, **210**, 269-276.

Rixhon, G., May, S.M., Engel, M., Mechernich, S.; Schroeder-Ritzrau, A., Frank, N., Fohlmeister, J., Boulvain, F., Dunai, T., Brückner, H. (2018). Multiple dating approach (14C, 230Th/U and 36Cl) of tsunami-transported reef-top boulders on Bonaire (Leeward Antilles) - Current achievements and challenges. *Marine Geology*, doi.org/10.1016/j.margeo.2017.03.007.

Rosengaus Moshinsky, M. and Sánchez Sesma, J. (1990). Gilbert: ejemplo de huracanes de gran intensidad. *Ingeniería Hidráulica en México*, **1**:13-36.

Rosengaus Moshinsky, M., Jiménez Espinosa, M. and Vázquez Conde, M.T. (2014). Atlas climatológico de ciclones tropicales en México. CENAPRED, México: 108 pp.

Scheffers, A.M., Engel, M., May, S.M.; Scheffers, S.R., Joannes-Boyau, R., Hänssler, E., Kennedy, K., Kelletat, D., Brückner, H.; Vött, A.; Schellmann, G.; Schäbitz, F.; Radtke, U.; Sommer, B.; Willershäuser, T.; Felis, T. (2014). Potential and limits of combining studies of coarse- and fine-grained sediments for the coastal event history of a Caribbean carbonate environment. In: *Sedimentary Coastal Zones from High to Low Latitudes: Similarities and Differences* (ED I.P. Martini). Geol. Soc. London Spec. Pub, **388**, 503-531.

Shaw, C.E. and Benson, L. (2015). Possible Tsunami Deposits on the Caribbean Coast of the Yucatán Peninsula. *Journal of Coastal Research*, **31**, 1306-1316.

SSN (2018). Catálogo de Sismos. Servicio Sismológico Nacional, México. http://www2.ssn.unam.mx:8080/catalogo/ (last conexión 14-02-2018).

Szabo, B.J., Ward, W.C., Weidie, A.E., and Brady, M.J., 1978. Age and magnitude of the late Pleistocene sea-level rise on the eastern Yucatan Peninsula. *Geology*, **6**, 713–715.

Terry, J.P., Lau, A.Y.A., Etienne, S. (2013). Reef-platform Coral Boulders - Evidence for High-energy Marine Inundation Events on Tropical Coastlines. Springer, Singapore, 105 pp.

Ward, W.C. (1985). Quaternary geology of the northeastern Yucatan Peninsula. In: *Geology and hydrogeology of the Yucatan and quaternary geology of the Northeastern Yucatan Peninsula*. (Eds W.C. Ward, A.E. Weidie, A.E. and W. Back) pp. 23-53. New Orleans Geological Society.

Weidie, A.E. (1985). Geology of the Yucatan Platform. In: *Geology and hydrogeology of the Yucatan and quaternary geology of the Northeastern Yucatan Peninsula.* (Eds W.C. Ward, A.E. Weidie, A.E. and W. Back) pp. 1-19. New Orleans Geological Society.

Figures

Figure 1; a) Location map of the boulder ridges; b) Boulder ridge at Punta Venado (PV). c) Boulders at eastern Cozumel. Sites: XT: Xcaret, PV: Punta Venado, PA: Paamul, XH: XpuHa, KA: Kantenah, PL: Palladium Resort, XC: Xcacel, CT: Caleta Tankah.

Figure 2. Agisoft photogrammetry of some boulders in the Akumal Sector. All of the measurements used in this study can be obtained from the 3D reconstructions.

Figure 3. Boulder transport histogram for the boulders recorded at the study sites (see Tables 1 and 2 for the boulder properties and pre-transport settings).

Figure 4. Model of a tsunami generated by an earthquake Mw 7.6 along Motagua fault showing predicted wave height in the studied area.

Figure 5. Post classic Maya remains SW XpuHa upper the boulder ridge.

Tables

Table 1. Height of the extreme wave (tsunami and storm) necessary to move the boulders listed.

Table 2. Minimum flow velocity and flow depth to initiate boulder transport in different transport modes and using different Froude numbers (F_r=1; F_r=1.5).

Sector	Boulder	a	b	c	Corrected vol.	Weight kg	Nott - JBB		Engel and May – JBB	
							Ht	Hs	Ht	Hs
Paamul	BPM1	1.89	1.39	0.51	0.66	1490	1.0	4.0	1.2	4.9
	BPM2	1.19	0.46	0.46	0.12	280	0.1	0.6	1.1	4.4
	BPM3	1.37	0.81	0.45	0.24	555	0.4	1.7	1.1	4.3
	BPM5	0.84	0.80	0.70	0.23	523	0.3	1.0	1.7	6.7
	BPM6	1.48	1.14	0.74	0.61	1389	0.5	2.0	1.8	7.1
	BPM7	1.72	0.82	0.49	0.34	769	0.4	1.6	1.2	4.7
	BPM8	1.57	0.98	0.55	0.41	941	0.5	2.0	1.3	5.2
	BPM9	2.70	2.60	1.07	3.68	8355	1.6	6.5	**2.6**	**10.2**
	BPM10	3.70	1.72	0.80	2.49	5663	1.1	4.3	1.9	7.6
	B2-3	1.52	1.09	0.64	0.52	1179	0.5	2.1	1.5	6.1
	B2-4	0.85	0.77	0.53	0.17	386	0.3	1.3	1.3	5.1
	B2-5	1.26	0.90	0.58	0.32	732	0.4	1.6	1.4	5.5
	BPM11	2.00	0.74	0.57	0.41	938	0.3	1.2	1.4	5.4
Xcacel	BXC4	1.24	0.60	0.56	0.20	463	0.2	0.8	1.3	5.3
	B2	1.20	0.65	0.61	0.23	529	0.2	0.8	1.5	5.8
	B6	1.80	0.93	0.77	0.63	1434	0.3	1.3	1.8	7.3
	BA12	1.82	1.00	0.84	0.75	1700	0.4	1.4	**2.0**	**8.0**
	BN1	1.90	1.00	0.75	0.70	1585	0.4	1.6	1.8	7.2
	BN3	0.90	0.58	0.40	0.10	232	0.2	1.0	1.0	3.8
	BN5	1.40	1.17	0.76	0.61	1385	0.5	2.0	1.8	7.3
	BN6	2.02	1.20	0.42	0.50	1132	0.9	3.7	1.0	4.0
Cozumel	BCZ5	1.50	0.97	0.51	0.36	825	0.5	2.1	1.2	4.9
	BCZ6	3.70	2.38	0.82	3.54	8032	1.9	7.4	2.0	7.8
	BCZ7	1.90	1.60	1.20	1.79	4058	0.6	2.4	**2.9**	**11.5**
	BCZ8	2.00	1.90	0.30	0.56	1268	2.4	9.8	0.7	2.9
	BCZ9	2.49	2.00	0.70	1.71	3877	1.5	5.9	1.7	6.7
Palladium	BPA1	1.96	0.91	0.87	0.76	1726	0.3	1.1	**2.1**	**8.3**
	BPA2	1.60	1.30	0.95	0.97	2198	0.5	2.0	**2.3**	**9.1**
	BPA3	1.84	0.93	0.77	0.65	1466	0.3	1.3	1.8	7.3
	BPA4	1.50	0.95	0.57	0.40	903	0.5	1.8	1.4	5.4
	BPA5	1.86	0.92	0.89	0.75	1694	0.3	1.1	**2.1**	8.5
	BPA7	1.10	0.55	0.50	0.15	336	0.2	0.7	1.2	4.8
	BPA8	3.90	1.45	0.57	1.58	3585	1.1	4.3	1.4	5.4
	BPA9	2.10	1.00	1.00	1.03	2336	0.3	1.2	2.4	9.5
	BPA10	2.60	1.65	1.08	2.27	5154	0.7	2.9	**2.6**	**10.3**
	BPA11	2.30	1.30	0.71	1.04	2361	0.7	2.7	1.7	6.8
Akumal	BAK2	2.32	1.32	0.49	0.74	1669	1.0	3.9	1.2	4.7
	BAK3	2.02	1.00	0.84	0.83	1887	0.4	1.4	**2.0**	**8.0**
	BAK4	1.47	1.00	0.87	0.63	1423	0.3	1.3	**2.1**	**8.3**
	BAK5	1.30	1.24	0.38	0.30	681	1.0	4.0	0.9	3.6
	BAK6	1.38	1.02	0.86	0.59	1346	0.4	1.4	**2.1**	**8.2**

Kantenah	BKAN1	2.10	0.86	0.76	0.67	1527	0.3	1.2	1.8	7.3
	BKAN2	1.24	0.90	0.47	0.26	583	0.5	1.9	1.1	4.5
	BKAN4	3.10	2.01	0.70	2.14	4852	1.6	6.2	1.7	6.7
	BKAN5	2.12	1.30	0.52	0.70	1594	0.9	3.6	1.2	5.0
	BKAN8	1.21	0.78	0.41	0.19	430	0.4	1.7	1.0	3.9
	BKAN9	2.30	2.10	0.51	1.21	2740	2.0	8.1	1.2	4.9
	BKAN10	2.70	1.56	1.00	2.06	4685	0.7	2.8	**2.4**	**9.5**

Boulder ID	Minimum Flow velocity to initiate boulder transport (m/s)				Minimum flow depth to initiate boulder transport (m)							
					F_r=1.0				F_r=1.5			
	sliding	rolling	saltation	lifting	slid.	roll.	saltat.	lift.	slid.	roll.	saltat.	lift.
BPM1	3.3	5.3	8.3	8.4	1.1	2.9	7.0	7.3	0.5	1.3	3.1	3.2
BPM2	2.0	2.3	7.9	8.0	0.4	0.6	6.3	6.6	0.2	0.2	2.8	2.9
BPM3	2.6	3.8	7.8	7.9	0.7	1.5	6.2	6.4	0.3	0.6	2.8	2.9
BPM5	2.6	3.2	9.7	9.9	0.7	1.1	9.6	10.0	0.3	0.5	4.3	4.4
BPM6	3.1	4.3	10.0	10.2	1.0	1.9	10.2	10.5	0.4	0.8	4.5	4.7
BPM7	2.6	3.7	8.1	8.3	0.7	1.4	6.7	7.0	0.3	0.6	3.0	3.1
BPM8	2.9	4.1	8.6	8.8	0.8	1.7	7.6	7.8	0.4	0.8	3.4	3.5
BPM9	4.6	7.2	12.0	12.2	2.1	5.3	14.7	15.3	0.9	2.3	6.5	6.8
BPM10	3.7	5.7	10.4	10.6	1.4	3.3	11.0	11.4	0.6	1.5	4.9	5.1
B2-3	3.0	4.3	9.3	9.5	0.9	1.9	8.8	9.1	0.4	0.8	3.9	4.1
B2-4	2.6	3.5	8.5	8.6	0.7	1.2	7.3	7.6	0.3	0.5	3.2	3.4
B2-5	2.8	3.8	8.8	9.0	0.8	1.5	8.0	8.3	0.3	0.7	3.5	3.7
BPM11	2.5	3.3	8.8	8.9	0.6	1.1	7.8	8.1	0.3	0.5	3.5	3.6
BXC4	2.3	2.7	8.7	8.8	0.5	0.8	7.7	8.0	0.2	0.3	3.4	3.5
B2	2.4	2.8	9.1	9.2	0.6	0.8	8.4	8.7	0.3	0.4	3.7	3.9
B6	2.8	3.6	10.2	10.4	0.8	1.3	10.6	11.0	0.4	0.6	4.7	4.9
BA12	2.9	3.7	10.6	10.8	0.9	1.4	11.6	12.0	0.4	0.6	5.1	5.3
BN1	2.9	3.8	10.1	10.2	0.9	1.5	10.3	10.7	0.4	0.7	4.6	4.8
BN3	2.2	3.0	7.3	7.5	0.5	0.9	5.5	5.7	0.2	0.4	2.4	2.5
BN5	3.1	4.3	10.1	10.3	1.0	1.9	10.5	10.8	0.4	0.9	4.6	4.8
BN6	3.1	5.0	7.5	7.7	1.0	2.5	5.8	6.0	0.4	1.1	2.6	2.7
BCZ3	2.8	4.5	5.1	5.2	0.8	2.1	2.6	2.7	0.4	0.9	1.2	1.2
BCZ4	3.0	4.9	6.6	6.7	0.9	2.5	4.4	4.6	0.4	1.1	2.0	2.0
BCZ5	2.8	4.2	8.3	8.4	0.8	1.8	7.0	7.3	0.4	0.8	3.1	3.2
BCZ6	4.3	7.0	10.5	10.7	1.9	5.0	11.3	11.7	0.8	2.2	5.0	5.2
BCZ7	3.7	4.8	12.7	13.0	1.4	2.4	16.5	17.1	0.6	1.1	7.3	7.6
BCZ8	3.5	5.7	6.4	6.5	1.3	3.3	4.1	4.3	0.6	1.5	1.8	1.9
BCZ9	4.0	6.4	9.7	9.9	1.6	4.2	9.6	10.0	0.7	1.9	4.3	4.4
BPA1	2.8	3.3	10.8	11.0	0.8	1.1	12.0	12.4	0.4	0.5	5.3	5.5
BPA2	3.3	4.4	11.3	11.5	1.1	2.0	13.1	13.5	0.5	0.9	5.8	6.0
BPA3	2.8	3.6	10.2	10.4	0.8	1.3	10.6	11.0	0.4	0.6	4.7	4.9
BPA4	2.8	4.0	8.8	8.9	0.8	1.6	7.8	8.1	0.4	0.7	3.5	3.6
BPA5	2.8	3.3	11.0	11.2	0.8	1.1	12.2	12.7	0.4	0.5	5.4	5.6
BPA7	2.2	2.7	8.2	8.4	0.5	0.7	6.9	7.1	0.2	0.3	3.1	3.2
BPA8	3.4	5.4	8.8	8.9	1.2	3.0	7.8	8.1	0.5	1.3	3.5	3.6
BPA9	3.0	3.4	11.6	11.8	0.9	1.2	13.8	14.3	0.4	0.5	6.1	6.3
BPA10	3.7	5.1	12.1	12.3	1.4	2.7	14.9	15.4	0.6	1.2	6.6	6.8
BPA11	3.3	4.8	9.8	10.0	1.1	2.4	9.8	10.1	0.5	1.0	4.3	4.5
BAK2	3.2	5.2	8.1	8.3	1.1	2.7	6.7	7.0	0.5	1.2	3.0	3.1
BAK3	2.9	3.7	10.6	10.8	0.9	1.4	11.6	12.0	0.4	0.6	5.1	5.3
BAK4	2.9	3.6	10.8	11.0	0.9	1.3	12.0	12.4	0.4	0.6	5.3	5.5
BAK5	3.1	5.1	7.2	7.3	1.0	2.6	5.2	5.4	0.4	1.2	2.3	2.4

BAK6	3.0	3.7	10.8	11.0	0.9	1.4	11.8	12.3	0.4	0.6	5.3	5.4
BKAN1	2.7	3.4	10.1	10.3	0.8	1.1	10.5	10.8	0.3	0.5	4.6	4.8
BKAN2	2.7	4.0	8.0	8.1	0.8	1.7	6.5	6.7	0.3	0.7	2.9	3.0
BKAN3	2.7	4.3	6.6	6.7	0.7	1.9	4.4	4.6	0.3	0.8	2.0	2.0
BKAN4	4.0	6.4	9.7	9.9	1.6	4.2	9.6	10.0	0.7	1.9	4.3	4.4
BKAN5	3.2	5.1	8.4	8.5	1.1	2.7	7.2	7.4	0.5	1.2	3.2	3.3
BKAN6	2.7	4.4	5.2	5.3	0.7	2.0	2.8	2.9	0.3	0.9	1.2	1.3
BKAN7	3.2	5.4	7.2	7.3	1.1	3.0	5.2	5.4	0.5	1.3	2.3	2.4
BKAN8	2.5	3.8	7.4	7.6	0.7	1.4	5.6	5.8	0.3	0.6	2.5	2.6
BKAN9	3.9	6.5	8.3	8.4	1.6	4.3	7.0	7.3	0.7	1.9	3.1	3.2
BKAN10	3.6	5.0	11.6	11.8	1.3	2.6	13.8	14.3	0.6	1.1	6.1	6.3

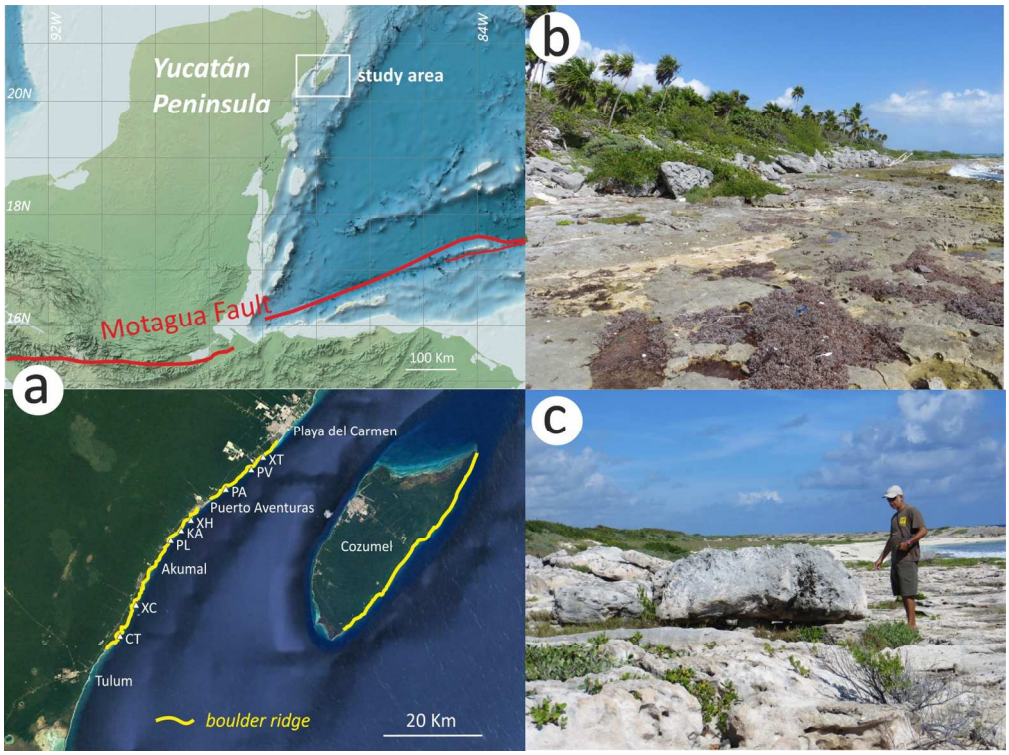

Figure 1; a) Location map of the boulder ridges; b) Boulder ridge at Punta Venado (PV). c) Boulders at eastern Cozumel. Sites: XT: Xcaret, PV: Punta Venado, PA: Paamul, XH: XpuHa, KA: Kantenah, PL: Palladium Resort, XC: Xcacel, CT: Caleta Tankah.

143x107mm (300 x 300 DPI)

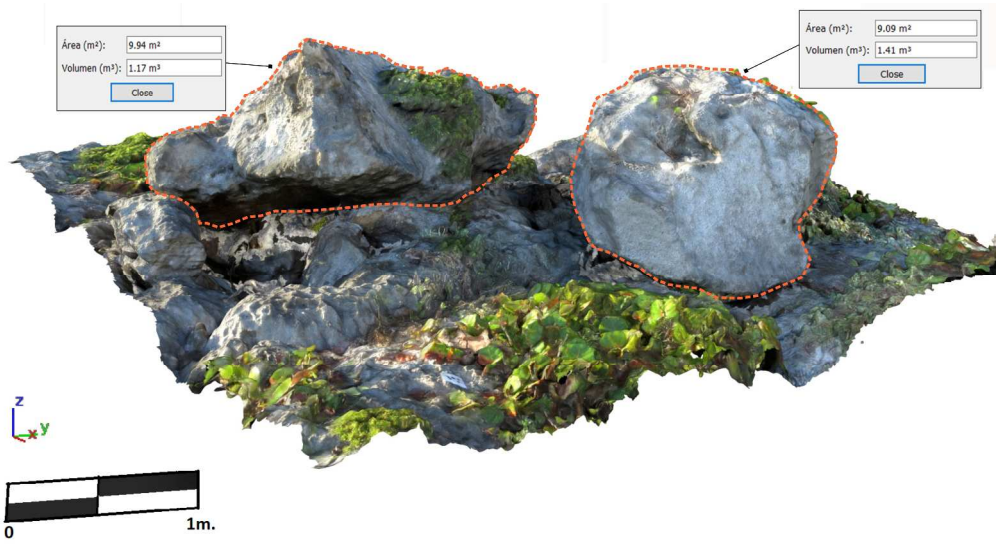

Figure 2. Agisoft photogrammetry of some boulders in the Akumal Sector. All of the measurements used in this study can be obtained from the 3D reconstructions.

376x204mm (300 x 300 DPI)

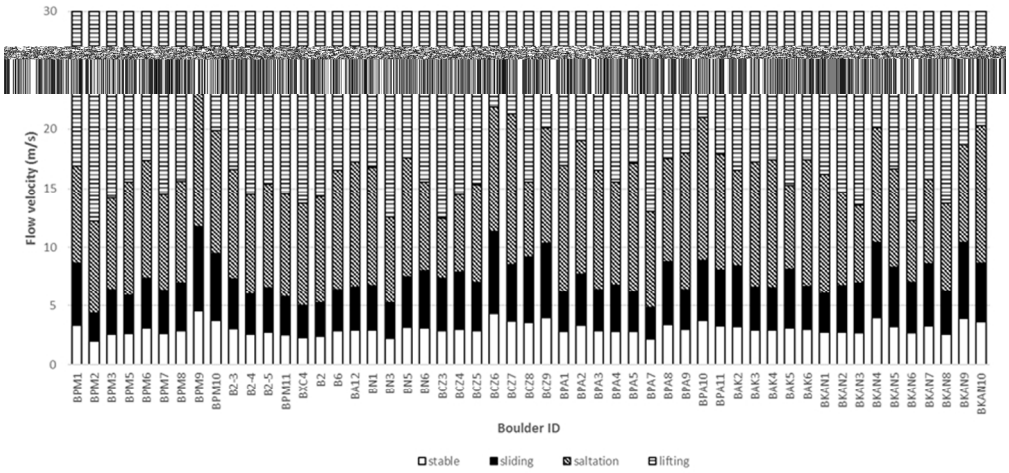

Figure 3. Boulder transport histogram for the boulders recorded at the study sites (see Tables 1 and 2 for the boulder properties and pre-transport settings).

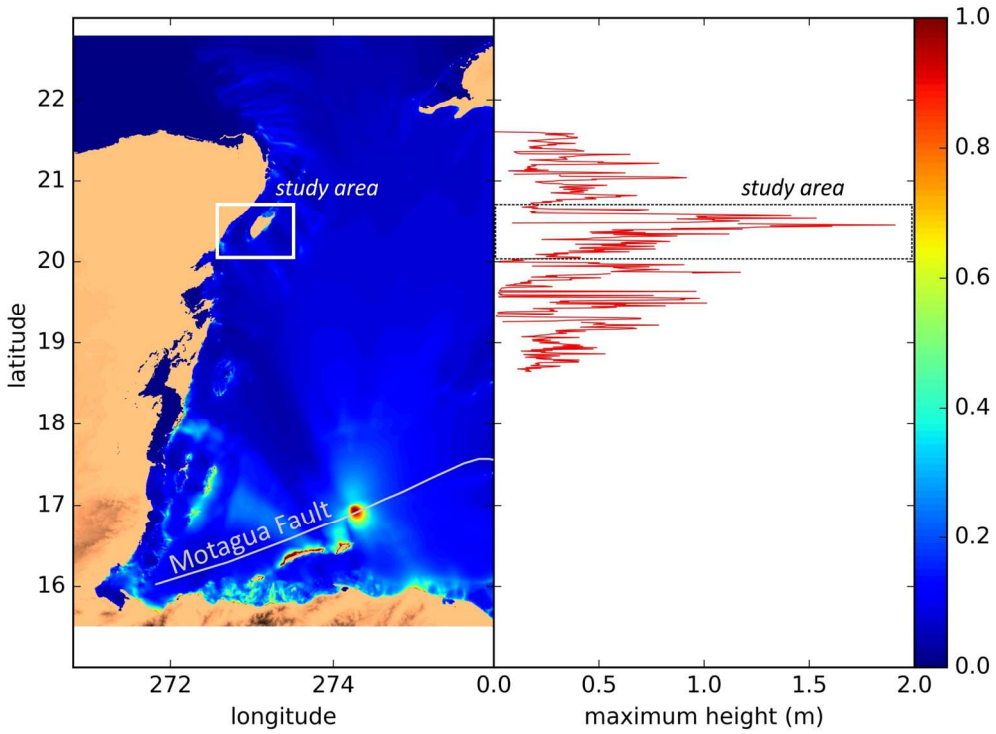

Figure 4. Model of a tsunami generated by an earthquake Mw 7.6 along Motagua fault showing predicted wave height in the studied area.

146x106mm (300 x 300 DPI)

Figure 5. Post classic Maya remains SW XpuHa upper the boulder ridge

397x298mm (180 x 180 DPI)